This article has been accepted for publication in a future issue of this journal, but has not been fully edited. Content may change prior to final publication. Citation information: DOI10.1109/TCDS.2023.3338460, IEEE Transactions on Cognitive and Developmental Systems

Sub-Band Cascaded CSP-based Deep Transfer Learning for Cross-Subject Lower Limb Motor Imagery Classification

Mingnan Wei, Rui Yang, *Member, IEEE*, Mengjie Huang, *Member, IEEE*, Jiaying Ni, Zidong Wang, *Fellow, IEEE*, and Xiaohui Liu

Abstract—Lower limb motor imagery (MI) classification is a challenging research topic in brain-computer interface (BCI) due to excessively close physiological representation of left and right lower limb movements in the human brain. Moreover, MI signals have severely subject-specific characteristics. The classification schemes designed for a specific subject in previous studies could not meet the requirements of cross-subject classification in a generic BCI system. Therefore, this study aimed to establish a cross-subject lower limb MI classification scheme. Three novel sub-band cascaded common spatial pattern (SBCCSP) algorithms were proposed to extract representative features with low redundancy. The validations had been conducted based on the lower limb stepping-based MI signals collected from subjects performing MI tasks in experiments. The proposed schemes with three SBCCSP algorithms have been validated with better accuracy and running time performances than other common spatial pattern (CSP) variants with the best average accuracy of 98.78%. This study provides the first investigation of a cross-subject MI classification scheme based on experimental stepping-based MI signals. The proposed scheme will make an essential contribution to developing generic BCI systems for lower limb auxiliary and rehabilitation applications.

Index Terms—Brain-Computer Interface, Motor Imagery Classification, Sub-Band Cascaded Common Spatial Pattern, Cross-Subject Transfer Learning, Deep Transfer Learning

1 Introduction

Brain-computer interface (BCI), which can establish an alternative and enhanced communication channel between the human brain and the external device, has demonstrated its great potential to be integrated with auxiliary and rehabilitation applications [1], [2], [3], [4]. Motor imagery (MI) signal is a physiological signal generated when the user imagines the movements of limbs. By analyzing the brain activation patterns, MI-based BCI can recognize the user's movement intention and then control the device with brain activities [5], [6].

Research into decoding upper limb MI classification BCI is developing rapidly. The lateralization of the upper limb representation area in the brain is relatively apparent in classifying the left and right upper limb MI tasks. However, the physiological representation areas for the left and right lower limbs are located within the interhemispheric fissure of the sensorimotor cortex and share the proximity spatially [7], [8]. Thus, the classification of left and right lower limbs MI is more challenging than the classification of upper limb MI. The lower limb MI classification is gaining increased attention from researchers [9], [10], [11].

From the literature, MI signals used for stepping classification can be categorized into foot-based MI signals, stepping-standing MI signals and stepping-based MI signals [12], [13], [14]. The most significant difference between the three signals is that the subjects perform the MI task differently, involving different body parts. The foot-based MI task asks subjects to imagine the movement of feet. However, the classification results are not ideal because the representation areas of the left and right foot are too close in the sensorimotor cortex [15], [16]. The low discrimination between signals limits the application effect of foot-based MI signals in stepping classification. For the stepping-standing MI classification, subjects need to imagine walking upright or stopping in place. The principle is similar to a brain-controlled switch, only focusing on the start and finish of the stepping tasks. Generally, the stepping-standing MI shows more accurate classification results than the foot-based MI [17], [18]. However, the stepping-standing MI classification suffers the disadvantage of limited application scope. The movement order of the stepping-standing MI task is usually pre-set and fixed. In this case, users cannot change the movement order and realize complex gait. The classification of stepping-based MI aims at the left and right

- *This research is partially supported by: National Natural Science Foundation of China (61603223), Jiangsu Provincial Qinglan Project, Suzhou Science and Technology Programme (SYG202106), Research Development Fund of XJTLU (RDF-18-02-30, RDF-20-01-18), Key Program Special Fund in XJTLU (KSF-E-34) and The Natural Science Foundation of the Jiangsu Higher Education Institutions of China (20KJB520034).*
- *Mingnan Wei is with School of Advanced Technology, Xi'an Jiaotong-Liverpool University, Suzhou 215123, China and School of Electrical Engineering, Electronics & Computer Science, University of Liverpool, Liverpool L69 3BX, United Kingdom.*
- *Rui Yang is with School of Advanced Technology, Xi'an Jiaotong-Liverpool University, Suzhou 215123, China and Research Institute of Big Data Analytics, Xi'an Jiaotong-Liverpool University, Suzhou 215123, China.*
- *Mengjie Huang and Jiaying Ni are with Design School, Xi'an Jiaotong-Liverpool University, Suzhou 215123, China.*
- *Zidong Wang and Xiaohui Liu are with Department of Computer Science, Brunel University London, Uxbridge, Middlesex UB8 3PH, United Kingdom.*
- *Corresponding authors: Rui Yang (R.Yang@xjtlu.edu.cn) and Mengjie Huang (Mengjie.Huang@xjtlu.edu.cn)*

This article has been accepted for publication in a future issue of this journal, but has not been fully edited. Content may change prior to final publication. Citation information: DOI10.1109/TCDS.2023.3338460, IEEE Transactions on Cognitive and Developmental Systems

stepping tasks, which involves the cooperative imagery of movements performed by multiple body parts, including the hip, thigh, calf, knee, foot, and toes. By comparison, the stepping-based MI signals include richer spatial characteristics of electroencephalogram (EEG) than the foot-based MI signals. The stepping-based MI signals can also satisfy more complex movement demands than the stepping-standing MI signals. Therefore, the stepping-based MI signals are more suitable for the lower limb stepping MI tasks than the other two.

In the literature, only two previous studies in 2017 and 2019 focused on the stepping-based MI signals [19]. The first study aimed to classify the EEG patterns of stepping-based MI tasks and obtained 86% classification accuracy through a model using filter bank common spatial pattern (FBCSP) and fuzzy support vector machine (FSVM) [14]. Based on the same EEG dataset, a detailed statistical analysis of the event-related desynchronization (ERD) and event-related synchronization (ERS) of stepping-based MI signals was conducted in the second study [19]. In addition to the EEG μ and β bands that play essential roles in the previous lower limb MI classification studies, the second study demonstrated that the θ band also provides valuable information for stepping-based MI classification. These two studies provide favorable evidence that stepping-based MI signals are suitable for lower limb stepping recognition and classification.

MI signals own the subject-specific, non-stationary, and time-varying characteristics [20], [21], [22]. The existing classification methods of MI signals were mainly designed for a single subject and did not meet the cross-subject classification requirement [14], [23]. The MI data re-collection and classification model re-training for the new subject could lead to extra body burden and time consumption [24], [25]. A cross-subject stepping-based MI classification scheme can improve the reuse rate of the classification model and significantly reduce the alignment time for new subjects. Therefore, the generic stepping-based MI classification is essential to developing commercial-level BCI for lower limb auxiliary and rehabilitation applications [26], [27]. Until now, there has been no relevant study on cross-subject classification based on stepping-based MI signals in the literature.

The most crucial step for the cross-subject MI classification model is to extract the common features of different subjects. The common spatial pattern (CSP) is one of the most widely used feature extraction algorithms in MI classification. CSP can extract the feature vectors with high discrimination from the multi-channel EEG signals [28]. Because the general CSP only targets a single wideband and may lead to insufficient feature extraction, the majority of CSP variants implement the extraction on multiple sub-bands [29]. However, the extraction on the narrow sub-bands may lead to features with low representativeness and high redundancy. Through the existing literature, the methods of current CSP variants to perform the feature selection can be divided into two classes, as shown in Fig. 1.

The first class of CSP variants displayed in Fig. 1 calculates the significance of each sub-band in various ways, thereby screening out the atypical sub-bands [30]. In contrast, the second class of CSP variants calculates the significance of each feature in various ways and screens out the

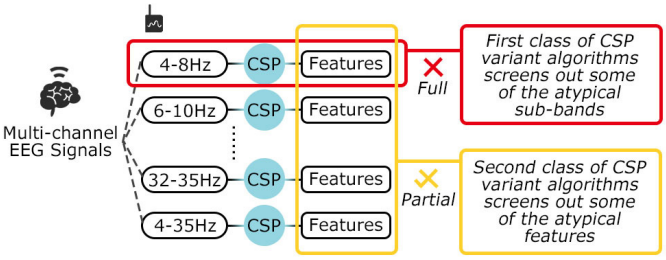

Fig. 1: Two classes of feature selection methods of the CSP variants

atypical features [31], [32]. Discarding atypical features or sub-bands can reduce the feature redundancy to some extent but may also discard some valuable information. Especially when dealing with the cross-subject problem with significant data distribution differences, these atypical features or sub-bands may vastly improve the classification performance. Moreover, current CSP variants do not implement feature refinement to improve the representativeness of features and decrease the number of features. Since the number of extracted features is much more than the discarded ones, excessive features in training may cause computing-inefficient and time-consuming classification. Therefore, an improved feature extraction algorithm that deeply extracts valuable information and compresses the number of multiple features is incredibly significant for the cross-subject MI classification.

Based on the analysis above, an investigation on generic cross-subject stepping-based MI classification was conducted in this paper. To the best of the authors' knowledge, no previous published work has presented such a problem. MI signals own severely subject-specific characteristics. Extracting the common features of different subjects is the biggest challenge of this cross-subject stepping-based MI classification. However, the existing CSP variants may have the disadvantages of discarding some atypical and low-value features without feature refinement, leading to the loss of partial classified information and the computing-inefficient classification. Therefore, three novel sub-band cascaded common spatial pattern (SBCCSP) algorithms were proposed in this paper for the cross-subject MI classification to deeply extract valuable information, improve the feature representativeness and compress the feature quantity. Three SBCCSP algorithms can respectively refine the individual features of each sub-band, aggregated features of all sub-bands, and both the individual features and the aggregated features. Therefore, the proposed SBCCSP can help achieve the cross-subject MI classification with feature refining and redundancy removal.

In consideration of the challenging problem of cross-subject stepping-based MI classification, the main contributions of this paper are summarized as follows: 1) three novel SBCCSP algorithms were proposed to extract features of MI signals with strong representativeness and low redundancy; 2) a novel cross-subject lower limb MI classification scheme based on stepping-based MI signals was proposed to improve the reuse rate of the classification model for new users. The stepping-based MI classification experiments in-

This article has been accepted for publication in a future issue of this journal, but has not been fully edited. Content may change prior to final publication. Citation information: DOI10.1109/TCDS.2023.3338460, IEEE Transactions on Cognitive and Developmental Systems

dicated that the SBCCSP algorithms perform better feature extraction than the CSP variants. The proposed cross-subject lower limb MI classification scheme can be significantly helpful in constructing generic BCI for the classification of stepping tasks.

The rest of this paper is organized as follows. Section 2 describes the preliminary knowledge for this paper. Section 3 introduces three novel SBCCSP and the scheme of cross-subject stepping classification. Section 4 elaborates on the acquisition experiments of stepping-based MI signals and discusses the experimental results of different methods. Finally, Section 5 concludes this paper and states the future work.

2 Preliminary Knowledge

In the lower limb MI classification, the general CSP and CSP variants algorithms are often used for feature extraction. The multi-band common spatial pattern (MBCSP) and FBCSP are two representative CSP variant algorithms that have shown remarkable performance and generalization ability in many studies [14], [19], [32]. To better discuss the improvement of the proposed SBCCSP algorithms, the following preliminary knowledge describes the mathematical principles and implementation methods of CSP, MBCSP and FBCSP algorithms.

2.1 Common Spatial Pattern

The general CSP algorithm aims to learn spatial filters from the EEG data for feature extraction such that the projected data from two classes would have maximal differences in their variances [34], [35]. Given the raw EEG matrix $E \in \mathbb{R}^{N\times P}$ with channel numbers N and sampling points P, R_1 and R_2 are the normalized covariance matrices of the two classes of signals, the combination of R_1 and R_2 can be decomposed as below:

$$R = R_1 + R_2 = U\Sigma U^T \tag{1}$$

where U is the eigenvector matrix, Σ is the diagonal matrix of eigenvalues (the eigenvalues are assumed to be sorted in descending order), and T is the symbol for transpose.

The whitening transformation P that equalizes the variances in the space spanned by each eigenvector in R can be computed as below:

$$P = \sqrt{\Sigma^{-1}}U^T \tag{2}$$

In CSP, the whitening transformation P is applied to R_1 and R_2, and the transformed matrices are shown in (3):

$$S_1 = PR_1P^T, S_2 = PR_2P^T \tag{3}$$

where S_1 and S_2 share the same eigenvectors.

By applying the principal component decomposition to S_1, S_2 can also be decomposed using the same eigenvector matrix and the sum of two corresponding eigenvalues is equal to one, as shown in (4):

$$if\ S_1 = B\Sigma_1 B^T, then\ S_2 = B\Sigma_2 B^T\ and\ \Sigma_1 + \Sigma_2 = I \tag{4}$$

where B is the eigenvector matrix, Σ_1 is the diagonal matrix of eigenvalue for the first class signal, Σ_2 is the diagonal matrix of eigenvalue for the second class signal, and I is the identity matrix.

The eigenvector corresponding to the maximum eigenvalue of S_1 causes the minimum eigenvalue of S_2 and vice versa. Therefore, the projection matrix of spatial filter W is obtained as below:

$$W = B^T P \tag{5}$$

By arranging the eigenvalue matrix in descending order, the screening projection matrix W' can be formed from the first m rows and last m rows of W, corresponding to the maximum and minimum eigenvalues. Then the EEG data E can be filtered by W', as shown in (6):

$$Z = W'E \tag{6}$$

where $Z \in \mathbb{R}^{2m\times P}$ is the projected matrix of E.

The projected matrix Z maximizes the difference in variances between two classes. Then the features f for classification are defined as below:

$$f = \log\left(\mathrm{var}\left(Z\right) / \sum_{i=1}^{2m} \mathrm{var}\left(Z_i\right)\right) \tag{7}$$

where the typical value of m is 1.

2.2 CSP Variants

2.2.1 Multi-Band Common Spatial Pattern

In MBCSP, the EEG signals are divided into different frequency sub-bands. Then the same CSP algorithm is performed on each sub-band to extract detailed features. After the extractions, the features from each sub-band are collected to generate the aggregated features for classification.

2.2.2 Filter Bank Common Spatial Pattern

In FBCSP, the signal is bandpass-filtered into multiple frequency bands, and the CSP features are extracted from each band. Then, a mutual information-based feature selection algorithm is adopted to select discriminative pairs of frequency bands automatically and corresponding CSP features [32], [33]. The mutual information I of the features of two sub-bands is shown in (8). Then the final decision is derived from the selected discriminative features from multiple frequency bands.

$$I(X;Y) = H(Y) - H(Y|X) \tag{8}$$

where X and Y are two groups of features, $H(X)$ and $H(Y)$ are the entropies of feature X and Y respectively, and $H(Y|X)$ is the conditional entropy of X and Y.

3 Proposed Methods

The proposed three novel SBCCSP algorithms and the novel cross-subject lower limb MI classification scheme based on stepping-based MI signals are elaborated in this section.

3.1 Sub-Band Cascaded Common Spatial Pattern

To refine the quality of extracted features, this paper proposes three novel types of SBCCSP by improving existing CSP variants. The cascaded spatial filters are respectively targeted for the individual features of each sub-band, the aggregated features of all sub-bands, and both the individual features and the aggregated features to realize the feature refinement.

This article has been accepted for publication in a future issue of this journal, but has not been fully edited. Content may change prior to final publication. Citation information: DOI10.1109/TCDS.2023.3338460, IEEE Transactions on Cognitive and Developmental Systems

3.1.1 Type I

The SBCCSP Type I algorithm is illustrated in Fig. 2, which is divided into four stages.

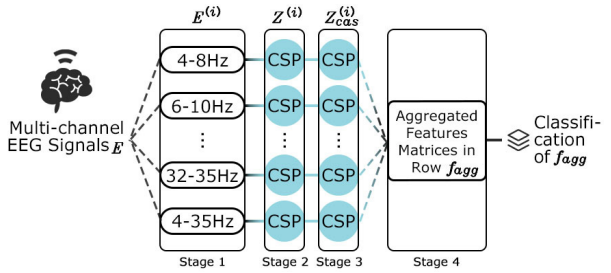

Fig. 2: Architecture of the proposed SBCCSP Type I algorithm

Algorithm 1: SBCCSP Type I

Input: signals E and number of sub-bands N_{sb}
Output: features f_{agg}

for *i=1; i≤N_{sb}; i++* **do**
  filter and divide E into the sub-band signals $E^{(i)}$;
  compute the first CSP projection matrix $W^{(i)}$ for $E^{(i)}$;
  generate the transformed signals $Z^{(i)}$ by filtering $E^{(i)}$ with $2m_1$ rows of $W^{(i)}$;
  compute the cascaded CSP projection matrix $W_{cas}^{(i)}$ for $Z^{(i)}$;
  generate the transformed signals $Z_{cas}^{(i)}$ by filtering $Z^{(i)}$ with $2m_2$ rows of $W_{cas}^{(i)}$ using (9);
  compute the features $f_{cas}^{(i)}$ for $Z_{cas}^{(i)}$ using (10);
end
combine $f_{cas}^{(i)}$ from all sub-bands in series to form the matrix of aggregated features f_{agg} using (11);
return the matrix of aggregated features f_{agg}

In stage 1, the bandpass filters divide the EEG signals E into numerous sub-bands $E^{(i)}$, including one wide sub-band (4-35Hz) and a group of overlapping sub-bands (e.g., 4Hz interval and 2Hz overlap). The first CSP and the cascaded CSP are introduced respectively in stage 2 and stage 3 to realize the refinement for the individual features of each sub-band, as Fig. 2 shows. The first CSP projection matrix $W^{(i)}$ is computed to implement the CSP extraction on $E^{(i)}$. The first m_1 and last m_1 rows of $W^{(i)}$ are selected to generate the transformed signals $Z^{(i)}$, as the $2m_1$ rows contain the most discriminative information. After the first CSP extraction, Type I conducts the cascaded CSP extraction on $Z^{(i)}$ in stage 3 to refine the valuable information. The cascaded CSP projection matrix $W_{cas}^{(i)}$ is computed to implement the cascaded CSP extraction on $Z^{(i)}$. The transformed signals of cascaded CSP $Z_{cas}^{(i)}$ are generated by $W_{cas}^{(i)}$ with $2m_2$ rows ($m_2 < m_1$) as shown in (9):

$$Z_{cas}^{(i)} = W_{cas}^{(i)} Z^{(i)} \tag{9}$$

By refining the cascaded CSP, the extracted information is condensed and re-filtered to improve the representativeness of valuable information and reduce the proportion of redundant information. The cascaded CSP features $f_{cas}^{(i)}$ are generated based on $Z_{cas}^{(i)}$ as shown in (10):

$$f_{cas}^{(i)} = \log\left(\mathrm{var}\left(Z_{cas}^{(i)}\right) / \sum_{j=1}^{2m_2} \mathrm{var}\left(Z_{cas(j)}^{(i)}\right)\right) \tag{10}$$

In stage 4, the algorithm combines the features $f_{cas}^{(i)}$ in series into the matrix of aggregated features f_{agg} as shown in (11).

$$f_{agg} = [f_{cas}^{(1)} \quad f_{cas}^{(2)} \quad \dots \quad f_{cas}^{(N_{sb})}] \tag{11}$$

where N_{sb} is the total number of sub-bands. The algorithm of SBCCSP Type I is summarized in Algorithm 1.

3.1.2 Type II

There are four stages in the SBCCSP Type II algorithm, as illustrated in Fig. 3. The first CSP and cascaded CSP are introduced respectively in stage 2 and stage 4 to realize the refinement of the aggregated features from all sub-bands.

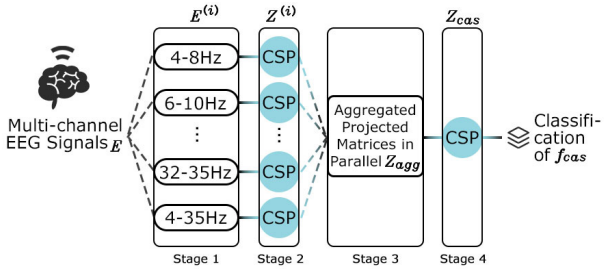

Fig. 3: Architecture of the proposed SBCCSP Type II algorithm

Algorithm 2: SBCCSP Type II

Input: signals E and number of sub-bands N_{sb}
Output: features f_{cas}

for *i=1; i≤N_{sb}; i++* **do**
  filter and divide E into the sub-band signals $E^{(i)}$;
  compute the first CSP projection matrix $W^{(i)}$ for $E^{(i)}$;
  generate the transformed signals $Z^{(i)}$ by filtering $E^{(i)}$ with $2m_1$ rows of $W^{(i)}$;
end
combine $Z^{(i)}$ from all sub-bands in parallel to form the aggregated transformed signals Z_{agg} using (12);
compute the cascaded CSP projection matrix W_{cas} for Z_{agg};
generate the transformed signals Z_{cas} by filtering Z_{agg} with $2m_2$ rows of W_{cas};
compute the features f_{cas} for Z_{cas};
return the features f_{cas}

The first two stages are the same as those of Type I, where E is divided into $E^{(i)}$ with the bandpass filters, and $W^{(i)}$ is obtained and used to generate $Z^{(i)}$. In stage 3, $Z^{(i)}$

This article has been accepted for publication in a future issue of this journal, but has not been fully edited. Content may change prior to final publication. Citation information: DOI10.1109/TCDS.2023.3338460, IEEE Transactions on Cognitive and Developmental Systems

from all sub-bands are combined in parallel to obtain the aggregated transformed signals Z_{agg} as shown in (12):

$$Z_{agg} = \begin{bmatrix} Z^{(1)} \\ Z^{(2)} \\ \cdots \\ Z^{(N_{sb})} \end{bmatrix} \tag{12}$$

In stage 4, W_{cas} is constructed by Z_{agg} and used to implement the refinement to generate Z_{cas}. Finally, the features f_{cas} are computed by Z_{cas}. The refinement of Type II is relatively comprehensive because the method integrates information from all sub-bands and re-filters redundant information. The number of classified features can be reduced, boosting the rapid convergence of training. To summarize, the algorithm of SBCCSP Type II is shown in Algorithm 2.

3.1.3 Type III

The SBCCSP Type III algorithm is an improved version of Type I and Type II and can be divided into five stages, as shown in Fig. 4. The first three stages inherit the Type I algorithm to implement the deep refinement for individual features of each sub-band. The last two stages inherit the Type II algorithm to implement comprehensive refinement on the aggregated features from all the sub-bands.

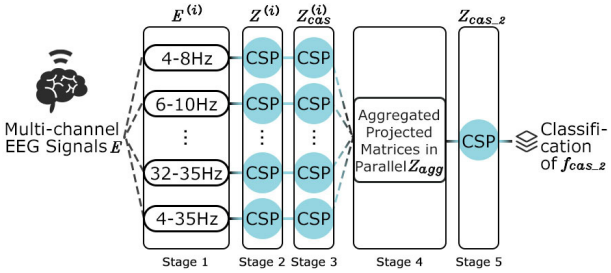

Fig. 4: Architecture of the proposed SBCCSP Type III algorithm

First of all, E is filtered and divided into $E^{(i)}$ in stage 1. Then the $W^{(i)}$ is computed using the CSP algorithm to obtain $Z^{(i)}$ in stage 2. In stage 3, $W^{(i)}_{cas}$ is obtained based on first cascaded CSP to obtain $Z^{(i)}_{cas}$. In stage 4, the $Z^{(i)}_{cas}$ are aggregated to form Z_{agg}. Then the projection matrix of the second cascaded CSP W_{cas_2} with $2m_3$ rows is computed and used to generate the transformed signals Z_{cas_2} in stage 5. Finally, the features f_{cas_2} are obtained by Z_{cas_2}.

Through the doubly cascaded CSP filtering, SBCCSP Type III can refine the valuable information of each sub-band, integrate the information of all sub-bands and reduce the number of features. To summarize, the algorithm of SBCCSP Type III is shown in Algorithm 3.

On the whole, the SBCCSP Type I focuses on the deep refinement of each sub-band and is suitable for the case of high redundancy in features within the same sub-band and low redundancy in features between different sub-bands. In contrast with Type I, Type II focuses on refining the aggregated features of the different sub-bands to integrate information from all sub-bands and eliminate redundant information. Combined with the advantages of Type I and Type II, Type III can implement the deep refinement of each sub-band and comprehensive refinement of different sub-bands.

Algorithm 3: SBCCSP Type III

Input: signals E and number of sub-bands N_{sb}
Output: features f_{cas_2}

for *i*=1; *i*≤N_{sb}; *i*++ **do**
  filter and divide E into the sub-band signals $E^{(i)}$;
  compute the first CSP projection matrix $W^{(i)}$ for $E^{(i)}$;
  generate the transformed signals $Z^{(i)}$ by filtering $E^{(i)}$ with $2m_1$ rows of $W^{(i)}$;
  compute the first cascaded CSP projection matrix $W^{(i)}_{cas}$ for $Z^{(i)}$;
  generate the transformed signals $Z^{(i)}_{cas}$ by filtering $Z^{(i)}$ with $2m_2$ rows of $W^{(i)}_{cas}$;
end
combine $Z^{(i)}_{cas}$ from all sub-bands in parallel to from the aggregated transformed signals Z_{agg};
compute the second cascaded CSP projection matrix W_{cas_2} for Z_{agg};
generate the transformed signals Z_{cas_2} by filtering Z_{agg} with $2m_3$ rows of W_{cas_2};
compute the features f_{cas_2} for Z_{cas_2};
return the features f_{cas_2}

3.2 Cross-Subject Lower Limb Motor Imagery Classification Scheme

In order to overcome the problem of cross-subject stepping MI classification, a novel classification scheme based on the stepping-based MI signals was proposed in this paper. As shown in Fig. 5, this scheme consists of five parts, including data preprocessing, data augmentation, data alignment, feature extraction, and model establishment. In addition to efficient cross-subject classification, the ability to achieve fast response was considered for the practical and real-time application scenarios. Based on the transfer learning (TL), the cross-subject scheme can use a small number of new subject samples to fine-tune the pre-trained classifier of other subjects, delivering high-performance classification and reducing the training cost for new subject use.

3.2.1 Data Preprocessing

The Butterworth bandpass filter and independent component analysis (ICA) were utilized to remove the outliers and artifacts in the data. By applying a 4-35Hz bandpass filter, the MI characteristics could be retained, and the non-physiological artifacts (∼50Hz) could be eliminated [36], [37], [38], [39]. The ICA was adopted to observe the independent components with the assistance of the IClabel and manually remove the physiological components, which profoundly interfere with the actual distribution of EEG signals [40], [41], [42].

3.2.2 Data Augmentation

Each trial of preprocessed EEG signals was divided into multiple data segments without any overlap to expand the sample size and avoid data leakage between the training set and test set. Based on past experimental experience, the overall reaction and computation time in the actual operation of the lower limb robot should be less than 1000ms to

This article has been accepted for publication in a future issue of this journal, but has not been fully edited. Content may change prior to final publication. Citation information: DOI10.1109/TCDS.2023.3338460, IEEE Transactions on Cognitive and Developmental Systems

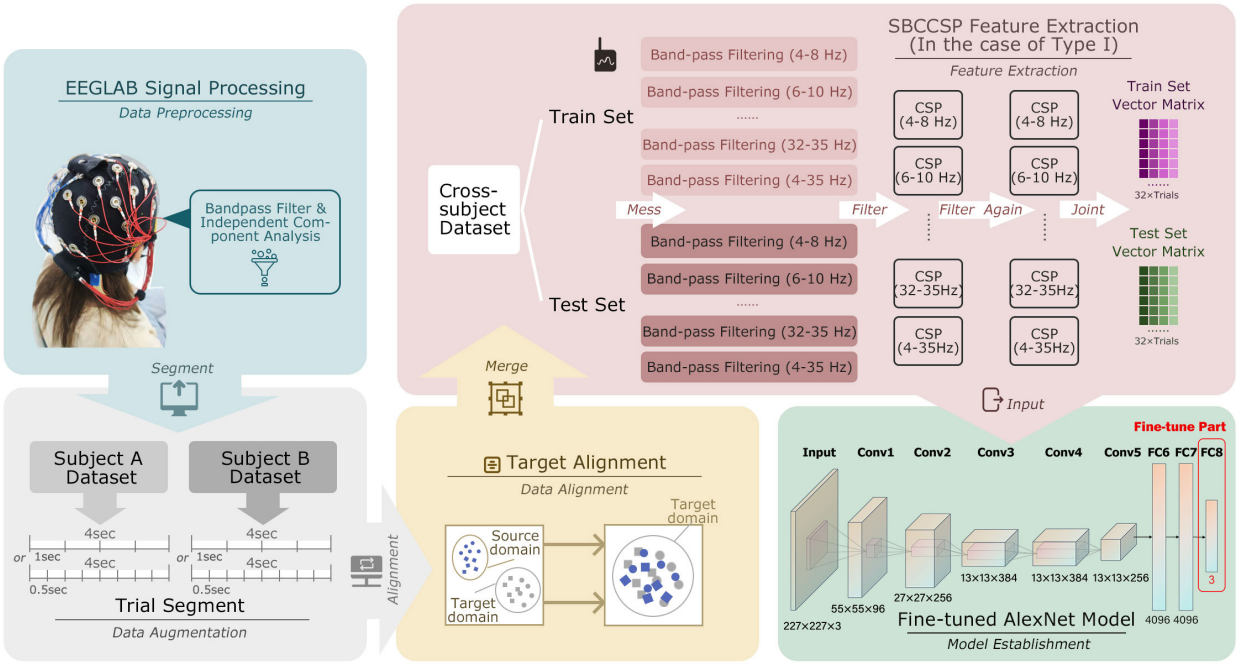

Fig. 5: Cross-subject lower limb MI classification scheme

meet an essential requirement under limited response time. Therefore, this scheme adopted the data segments of 500ms and 1000ms as the short time windows.

3.2.3 Data Alignment

Target alignment (TA) was adopted to reduce the distribution differences between two datasets [43]. Assuming the data of subject A is in the source domain $\mathcal{D}_s$ and the data of subject B is in the target domain $\mathcal{D}_t$, TA maps the data in $\mathcal{D}_s$ to data in $\mathcal{D}_t$ to obtain minimized difference in covariance matrix and consistent data distribution.

3.2.4 Feature Extraction

The proposed SBCCSP algorithms were implemented to extract the common features of cross-subject signals. After CSP extractions on multiple sub-bands, three types of SBCCSP algorithms could be selected to implement the cascaded CSP extractions based on Algorithm 1, 2 or 3 respectively. The SBCCSP could extract features with low redundancy to refine valuable information and compressing feature number.

3.2.5 Model Establishment

Deep transfer learning (DTL) aimed at deploying deep learning for transfer learning, which transferred potentially transferable knowledge from other fields into the target field to improve classification performance and save retraining costs. DTL-based AlexNet had shown excellent generalization ability and proven effective in many fields, including upper limb MI classification [44], [45], [46], [47], [48]. In addition, DTL-based AlexNet was ideally suited for practical and real-time application scenarios. Its lightweight structure to conduct the fast response helped build the efficient time series classifier. Therefore, DTL-AlexNet was adopted as the final classifier in the cross-subject lower limb MI classification scheme.

To transform this AlexNet model for the stepping-based MI classification, the DTL method retained the front layers of the pre-trained AlexNet because these layers can be treated as a versatile feature extractor that had already learned to extract informative and robust features. The last three layers (two fully connected layers and one output layer with 2048 classes) of AlexNet were rebuilt with three new layers (two fully connected layers and one output layer with MI task class number), and the weights were fine-tuned and updated with the extracted features. The final parameters of the pre-trained AlexNet model were optimized and determined by the performance comparisons in classification.

4 Experiment and Results Analysis

Experiments were designed to collect lower limb stepping-based MI signals from subjects performing MI tasks. Then the effectiveness of the SBCCSP algorithms and cross-subject classification scheme is verified by the acquired MI data.

4.1 Ethics

This research has been approved by University Ethics Committee of Xi'an Jiaotong-Liverpool University with proposal number EXT20-01-07 on March 31 2020. Prior to the experiments, the subjects read, and when they agreed, signed the consent form prior approved by the University Ethics Committee of Xi'an Jiaotong-Liverpool University.

4.2 Experiment Design

4.2.1 Subjects

Six able-bodied subjects (two males and four females aged 22-35 years) with normal or corrected vision participated in

This article has been accepted for publication in a future issue of this journal, but has not been fully edited. Content may change prior to final publication. Citation information: DOI10.1109/TCDS.2023.3338460, IEEE Transactions on Cognitive and Developmental Systems

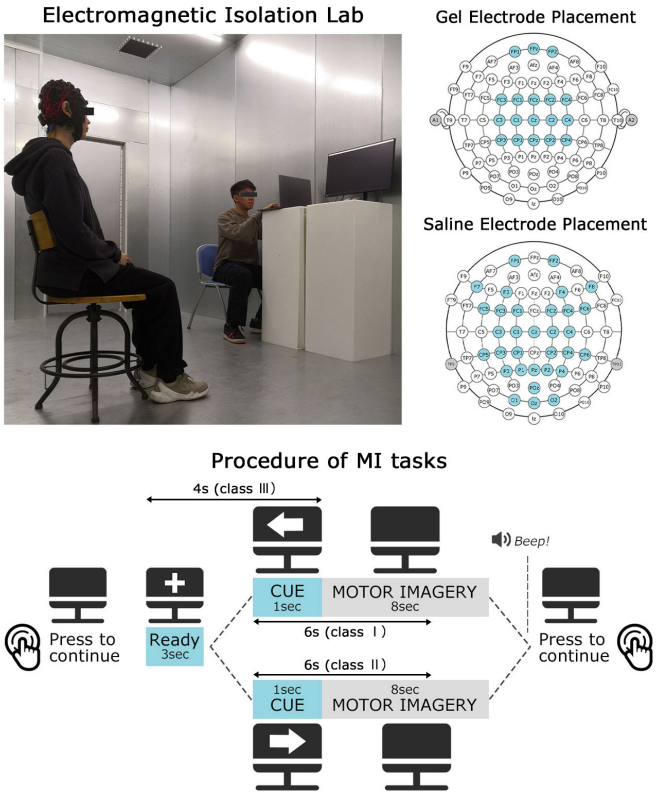

Fig. 6: Experiment setup in electromagnetic isolation lab and MI task procedure

the experiments. All subjects had no history of neurological disease and had not received any training related to regulating brain rhythm. Before the experiments, the informed consent form of each subject was obtained for the study. The specific experimental procedures and MI tasks were explained in detail to the subjects in advance.

4.2.2 *Experiment Setup*

The experiment setup is displayed in Fig. 6. The experiments were conducted in a specially designed electromagnetic isolation lab to minimize the effect of noise or electromagnetic disturbance. Metal isolation walls surrounded the lab, and the internal power supply and lighting were filtered. Two similar experiments with different EEG acquisition devices were designed to extensively verify the performances of the proposed methods and comprehensively assess the methods for the multiple acquisition devices. The EEG acquisition devices used in the experiments were Emotiv EPOC Flex Gel Kit and Emotiv EPOC Flex Saline Kit with a sampling rate of 128 Hz. The difference was that different conductive media (saline and conductive paste) needed to be used between the scalp and the electrode to obtain acceptable contact and reduce the impedance. With quick setup, high comfort, and convenient cleaning, saline electrode acquisition devices were suitable for a wide range of convenient application scenarios. Since the saline was easy to evaporate and flow, the saline electrode acquisition devices needed to be replenished frequently to ensure the stability of signal acquisition. In contrast, the gel electrodes had a better signal-to-noise ratio and transmission signal than saline electrodes, which can reduce the interference of artifacts and maintain excellent signal quality. However, the cumbersome setup limited the massive application of saline electrode acquisition devices. After the impedance check before the experiment, the devices utilized Bluetooth to connect with the computer to realize real-time data collection.

The first round of experiments was performed by two subjects and recorded using the Emotiv EPOC Flex Gel Kit. The electrodes for EEG acquisition in the experiment were mainly placed in the frontal area (FPz, FP1, FP2) and the central area (FCz, FC1, FC2, FC3, FC4, Cz, C1, C2, C3, C4, CPz, CP1, CP2, CP3, CP4) as shown in Fig. 6. This placement is because the physiological representation area of lower limb MI representation is mainly located within the interhemispheric fissure of the sensorimotor cortex. In addition, the frontal lobe is the area with the most dopamine-sensitive neurons to generate conscious thoughts and decisions, and it is responsible for the decision-making of limb movements [49], [50]. Researchers have focused on the relationship between this area and lower limb MI because the nature of MI tasks is the decision generation [51], [52]. The placement of electrodes in this experiment followed the international 10-20 system [53]. Besides, the reference electrodes are placed at the bilateral earlobes A1 and A2 on both sides.

To further explore the adaptation ability of proposed methods for the cross-subject classification under various devices and different electrode distributions, the second round of experiments was conducted on four subjects using the Emotiv EPOC Flex Saline Kit. The saline electrodes were located in the frontal, central, parietal and occipital areas, including FP1, FP2, F3, F4, F7, F8, FC1, FC2, FC3, FC4, FC5, FC6, Cz, C1, C2, C3, C4, CP1, CP2, CP3, CP4, CP5,

This article has been accepted for publication in a future issue of this journal, but has not been fully edited. Content may change prior to final publication. Citation information: DOI10.1109/TCDS.2023.3338460, IEEE Transactions on Cognitive and Developmental Systems

CP6, Pz, P1, P2, P3, P4, POz, O1, Oz, O2 shown in Fig. 6. The reference electrodes were adjusted from the bilateral earlobes to bilateral mastoid TP9 and TP10.

4.2.3 Motor Imagery Tasks

The procedure of MI tasks for each trial is shown in Fig. 6. A ready sign '+' was displayed in the screen center for 3 seconds to indicate the start of preparation and inform the subject to get ready. Then a random MI task cue (left or right arrow) was displayed for 1 second to indicate the stepping-based MI of left or right stepping. After the arrow was displayed for 1 second and disappeared, the subject performed the corresponding MI task for 8 seconds. The subject stopped the task for a short rest and got ready for the subsequent trial when hearing a beep sound.

According to the completion status and fatigue status of the subject, the experimenter adjusted the rest time interval (4-8 seconds). Subjects performed the left and right stepping-based MI tasks multiple times, and there were 80 trials and 40 trials collected for each subject in gel and saline electrode experiments. The subsequent studies were conducted on these acquired MI data.

4.2.4 Data Processing

The data preprocessing steps were implemented in EEGLAB toolbox [54], such as bandpass filtering and ICA decomposition. Firstly, the raw signals were filtered by a bandpass filter to retain the 4-35Hz signals. The next task was to extract the trials of left and right stepping-based MI tasks from the signals. To collect the signals before and during the MI tasks, the range of each trial was 1 second before and 5 seconds after the disappearance of the MI task symbol, as shown in Figure 6. During the 1 second before the disappearance of the MI task symbol, the subject did not conduct the MI task and was in a relatively calm and stable state. The baseline correction regarded the EEG activity during the calm state as a baseline, subtracted the mean value within this 1 second with all data in each trial and corrected all trials to have a similar starting point and prevent the data drift. The left and right stepping-based MI data collected during the MI period were respectively labeled with class I ('1') and class II ('2') displayed in Fig. 6. In the actual lower limb movement, there are many non-motion states in addition to left and right stepping. As shown in Fig. 6, the range of 4 seconds before the disappearance of the MI task symbol was regarded as the idle (non-MI) state and labeled with class III ('3'). The idle state was set better to simulate the classification of lower limb MI tasks and test the performance of the proposed methodologies. The idle state was set better to simulate the classification of lower limb MI tasks and test the performance of the proposed methodologies. Furthermore, the ICA was used to decompose the data into multiple independent components, remove the physiological components with the help of the IClabel and reconstruct the data with the retained components. Since the EEG data of each subject was interfered with by different factors, the ICA was separately used for each subject to eliminate the non-EEG components of this subject's data effectively.

For the data of '1' and '2', the last 4 seconds of the trials were chosen to respectively divide into the multiple data segments of 500ms and 1000ms sizes without any overlap. The reason was that the subjects in this range fully engaged in the stepping-based MI tasks with the few interferences of visual stimulation of MI cue and fatigue of repetitive MI tasks. Based on the past experimental experience, there were no exceeding 100mV amplitudes for the standard cognitive activity data, so the data segments above this threshold were caused by other actions, considered heavily contaminated and excluded from the data. Since removing the multiple heavily contaminated data segments from the same trial resulted in the loss of a large amount of MI characteristic information, these trials with multiple heavily contaminated data segments were directly rejected. For the gel electrode data, there were 550 and 275 samples per class for the 500ms and 1000ms segment sizes. The 500ms and 1000ms data of saline electrode experiments contained 540 and 270 samples per class. Similarly, the 2 seconds between the first second and the third second of the trials of '3' were chosen and divided into segments with sizes of 500ms and 1000ms to ensure consistent sample quantity for the three classes. The final data matrices consisted of three dimensions representing the numbers of data points, channels and samples. The 500ms and 1000ms data matrices of the gel electrode experiments were $64\times32\times1650$ and $128\times32\times825$, and the 500ms and 1000ms data matrices of saline electrode experiments were $64\times18\times1620$ and $128\times18\times810$. To minimize the distribution differences of the multi-subject data, TA was used for the data alignment to generate the cross-subject data.

4.2.5 Classifier Training

Since general spatial filters were designed for the two-class classification task, this paper adopted three spatial filters to realize the three-class classification, as there were three classes: left stepping-based MI ('1'), right stepping-based MI ('2') and idle state ('3'). $2m$ rows of each spatial filter for any two-class classification were selected to form the three-class classification CSP filter with a total of $6m$ rows. Based on experimental experience, the optimal value of m_1, m_2 and m_3 were determined by exhaustive performance comparisons on the test accuracies. Finally, the Type I scheme set m_1 and m_2 as 3 and 2, the Type II scheme set m_1 and m_2 as 3 and 16, and the Type III scheme set m_1, m_2 and m_3 as 4, 3 and 16. To compare with the SBCCSP schemes, the common CSP, MBCSP and FBCSP schemes were applied, where m was set as 2 based on the comparisons. The feature matrices were converted into gray-scale images by normalizing the values of the matrices and generating the images with values in the range 0 (black) to 1 (white). Then, the gray-scale images were colored by the pseudo-color tool to generate the RGB color images and re-scaled into 277×277 pixels, following the required scale of AlexNet. The pre-trained AlexNet was deployed to carry out the final classification as a DTL approach. This study adopted several rounds of performance comparisons to test the performance of each parameter under different values and their overall combination performance. Through the exhaustive performance comparisons in classification, the final parameters of the pre-trained AlexNet model were optimized and set as follows: the stochastic gradient descent method was selected as the optimizer, the mini-batch size was set to 3, the epoch maximum was set to 4, and the initial learning rate was set to 0.00004. The programming language adopted in this

This article has been accepted for publication in a future issue of this journal, but has not been fully edited. Content may change prior to final publication. Citation information: DOI10.1109/TCDS.2023.3338460, IEEE Transactions on Cognitive and Developmental Systems

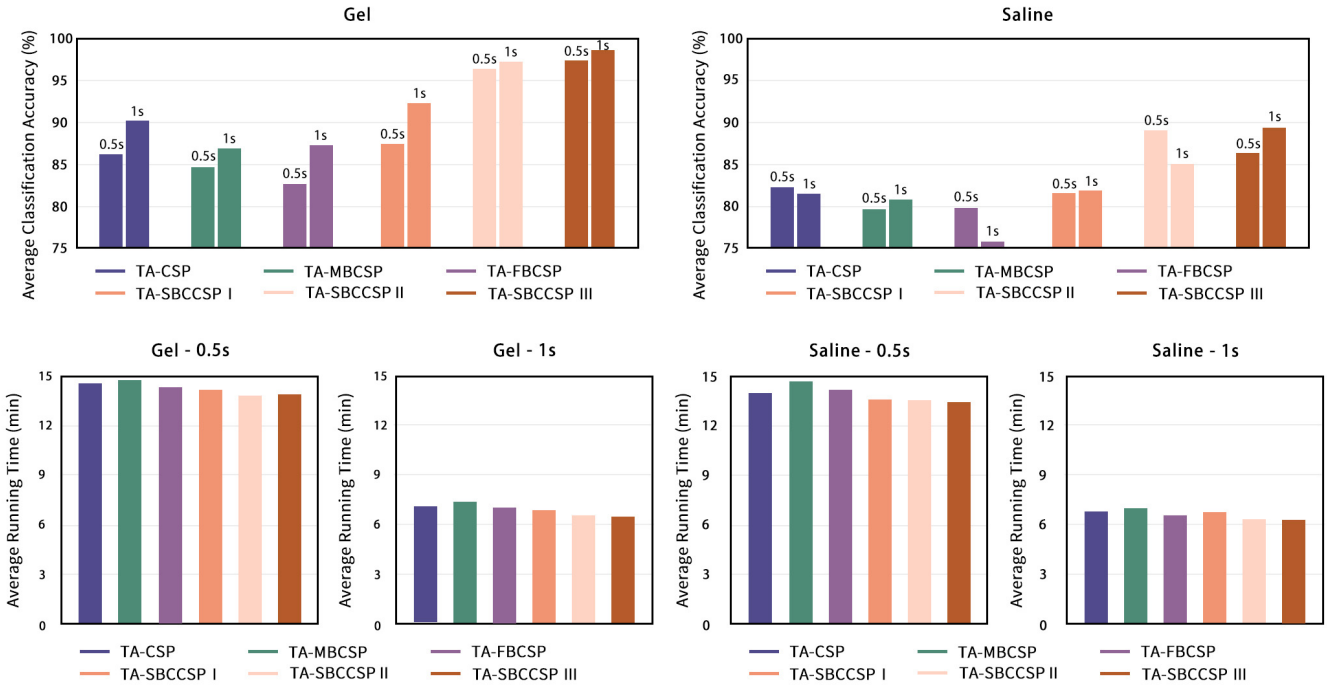

Fig. 7: Classified performance of schemes for all subjects in gel and saline electrode experiments of 500ms and 1000ms data

paper was Matlab, and the hardware parameters were Intel Xeon CPU E5-2678 v3, Nvidia GeForce Titan RTX GPU 24GB, and 64GB RAM.

4.3 Results and Analysis

The performances of the three TA-SBCCSP-DTL schemes and other comparative schemes on the cross-subject data with different data segment sizes and data are displayed from Fig. 7 to Fig. 9. Fig. 7 illustrates the performances of the schemes under the cross-subject gel electrode and saline electrode data for all subjects. In the cross-subject data, each subject's data was respectively shuffled and aggregated into two parts of the training set and testing set in a 7:3 ratio. Therefore, the training and testing data were not mixed up among the subjects. The average classification accuracies and average running time of the schemes were the mean values of three times. It can be observed that most schemes under 1000ms achieved better classification performance than those under 500ms because the schemes could extract more classified information from the data with a larger time interval. In contrast with the 500ms data, the 1000ms data contained the longer EEG signal duration and more abundant stepping-based MI feature information, which was more available to extract the high-discrepancy features and realize more efficient classifications. Furthermore, most schemes based on the proposed SBCCSP I/II/III algorithms achieved better average classification accuracies and running time than those based on CSP, MBCSP, and FBCSP algorithms in both 500ms and 1000ms data segments. The results proved that the SBCCSP algorithms had the generalization ability for different data segments. In addition, the classification accuracies of gel electrode data were generally better than those of saline electrode data. The main reason was that the gel electrodes had better electrical conductivity, signal-to-noise ratio, and stable connection than the saline electrodes, which can reduce the interference of artifacts and maintain excellent signal quality. Since the gel electrodes can collect cleaner and more accurate data than the saline electrodes, the schemes generally achieved better classification accuracies in the gel electrode data than in the saline electrode data. Whether 500ms or 1000ms data segments and gel electrode data or saline electrode data, most schemes based on the proposed SBCCSP I/II/III algorithms achieved better average classification accuracies and running time than those based on CSP, MBCSP, and FBCSP algorithms. Meanwhile, the performances of TA-SBCCSP II and TA-SBCCSP III schemes are better than other schemes, among which the average accuracies of 500ms and 1000ms data segments of gel electrode data and saline electrode data were more than 95% and 85%. Moreover, most schemes adopting three SBCCSP algorithms could shorten the running time compared with those adopting other feature extraction algorithms. Significantly, the TA-SBCCSP III scheme achieved the best performance for most classifications. In the saline electrode experiments of the 1000ms data segment, the scheme of SBCCSP III realized the best average accuracy of 98.78% and the best average running time of 6 minutes and 25 seconds.

The study adopted the paired T-test to compare whether the proposed three SBCCSP algorithms differ significantly from the existing CSP, MBCSP, and FBCSP algorithms. First, the processed data was divided into training and testing parts in a 7:3 ratio. All the schemes were trained with the same stochastic model seed five times to obtain the five sets of accuracies on the test data for six schemes. Based on the five sets of accuracies, TA-CSP, TA-MBCSP, and TA-FBCSP were respectively regarded as the baseline to compute the

This article has been accepted for publication in a future issue of this journal, but has not been fully edited. Content may change prior to final publication. Citation information: DOI10.1109/TCDS.2023.3338460, IEEE Transactions on Cognitive and Developmental Systems

TABLE 1: P values of T-test for all subjects in gel and saline electrode experiments of 500ms and 1000ms data segments (Note: Bold numbers represent the significant differences)

Scheme \ Data	Gel - 0.5s	Gel - 1s	Saline - 0.5s	Saline - 1s
TA-SBCCSP I (Baseline: TA-CSP)	**0.004252811**	**2.59578E-06**	0.654040021	**0.002507451**
TA-SBCCSP II (Baseline: TA-CSP)	**1.59489E-10**	**3.10365E-10**	**1.69293E-11**	**9.77561E-09**
TA-SBCCSP III (Baseline: TA-CSP)	**1.49E-10**	**3.57627E-11**	**3.82111E-09**	**3.29764E-11**
TA-SBCCSP I (Baseline: TA-MBCSP)	**5.57223E-06**	**1.5093E-08**	**2.09516E-06**	**2.06288E-05**
TA-SBCCSP II (Baseline: TA-MBCSP)	**3.0631E-11**	**1.00983E-10**	**3.55575E-09**	**4.22746E-09**
TA-SBCCSP III (Baseline: TA-MBCSP)	**3.07222E-11**	**3.96607E-11**	**1.1883E-10**	**3.95392E-11**
TA-SBCCSP I (Baseline: TA-FBCSP)	**2.11281E-09**	**1.99238E-08**	**3.97291E-06**	**1.54971E-09**
TA-SBCCSP II (Baseline: TA-FBCSP)	**1.45962E-13**	**2.20678E-11**	**1.5428E-10**	**2.65824E-11**
TA-SBCCSP III (Baseline: TA-FBCSP)	**2.3801E-13**	**8.34683E-11**	**5.01521E-09**	**2.45444E-12**

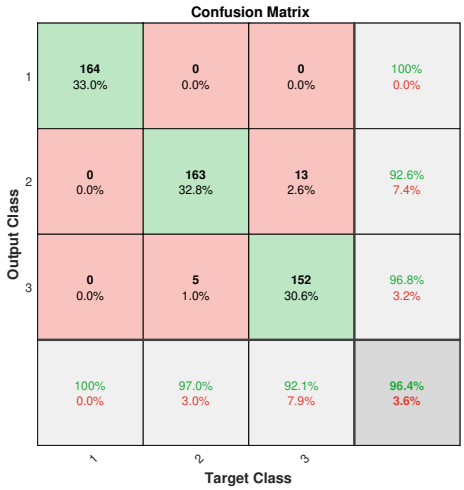

(a) Gel electrode experiments of 500ms data

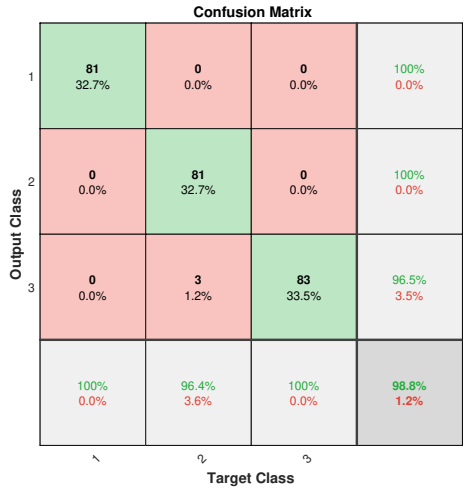

(b) Gel electrode experiments of 1000ms data

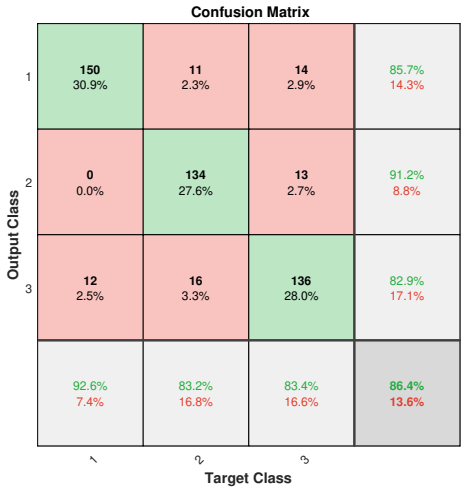

(c) Saline electrode experiments of 500ms data

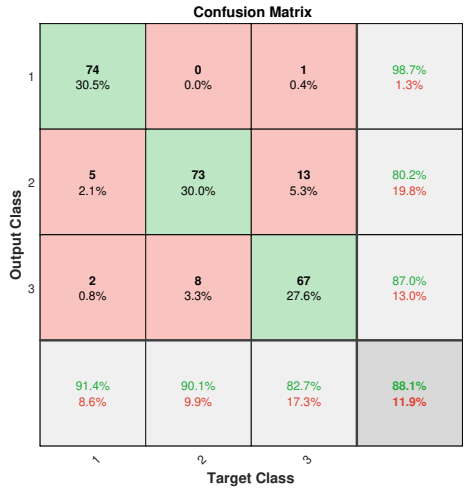

(d) Saline electrode experiments of 1000ms data

Fig. 8: Confusion matrices of TA-SBCCSP III schemes for all subjects in gel electrode experiments and saline electrode experiments of 500ms and 1000ms data segments

This article has been accepted for publication in a future issue of this journal, but has not been fully edited. Content may change prior to final publication. Citation information: DOI10.1109/TCDS.2023.3338460, IEEE Transactions on Cognitive and Developmental Systems

one-to-one P values with the proposed TA-SBCCSP I/II/III. All the results of the paired T-test are listed in Table 1. For multiple data with different data segments, almost all the P values (the bold) of the SBCCSP schemes were smaller than 0.01 in Table 1, indicating the performances of the proposed SBCSSP algorithms were statistically significantly better than those of the baseline algorithms of CSP, MBCSP, FBCSP. Furthermore, the TA-SBCCSP III scheme mostly achieved the most significant difference.

Due to the most effective classification, the confusion matrices of TA-SBCCSP III schemes for all subjects in gel electrode and saline electrode experiments of 500ms and 1000ms data segments are computed and displayed, as shown in Fig. 8. The rows and the columns corresponded to the predicted class (output class) and the proper class (target class). The diagonal cells and the off-diagonal cells corresponded to correctly classified features and incorrectly classified features. The number of features and the percentage of the total features were shown in each cell. The row at the bottom of the matrix showed the percentages of all the features belonging to each class that were correctly and incorrectly classified, called true positive rate (TPR) and false negative rate (FNR), respectively. The fourth column of the matrix showed the percentages of the predicted features in each class, which were correctly and incorrectly classified, called positive predictive value (PPV) and false discovery rate (FDR), respectively. For the classifications, the SBCCSP III obtained excellent accuracies from 86.4% to 98.8%. Class I (left stepping) had the highest mean TPR of 96% and the mean PPV of 96.1%, while class III (idle state) had the lowest mean TPR of 89.55% and the mean PPV of 90.8%. In addition, class I was most likely classified as class III, class II was easily mistaken for class III, and class III was most easily confused with class II. Compared with the cross-subject classifications on left and right stepping tasks, it was more challenging for the SBCCSP III scheme to recognize the idle state task efficiently.

Like Fig. 7, the average accuracies among all schemes for the target subject on the 500ms and 1000ms data segments are displayed in Fig. 9. Unlike the classification for all subjects with the training and testing ratio of 7:3, the schemes for the target subject were trained by the 5%-30% target subject's samples and all other subjects' samples, and tested by the rest of the target subject's samples. Choosing the different training and testing sets aimed to explore the cross-subject adaptation of the proposed methods for a new subject. When the ratio of the target subject's samples for training was small, the schemes based on the SBCCSP II and SBCCSP III algorithms had better average accuracies for each target subject compared with other schemes. With the

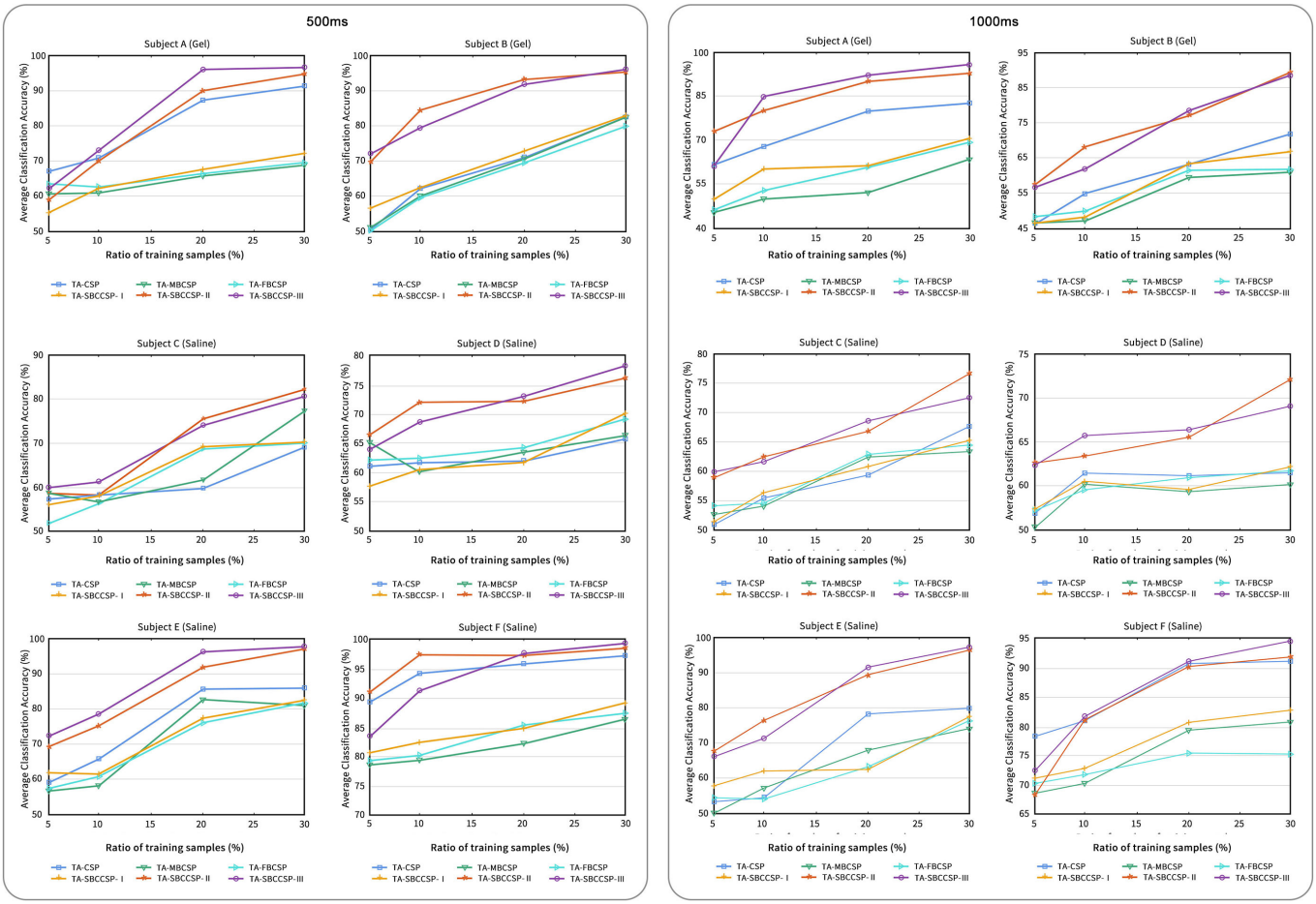

Fig. 9: Classification accuracies of different schemes in gel and saline electrode experiments with different ratio of training samples

This article has been accepted for publication in a future issue of this journal, but has not been fully edited. Content may change prior to final publication. Citation information: DOI10.1109/TCDS.2023.3338460, IEEE Transactions on Cognitive and Developmental Systems

increase in the ratio, the average accuracies of all schemes went up substantially and the accuracies of TA- SBCCSP II and TA-SBCCSP III schemes can exceed those of other schemes by about 10%. In most cases, the schemes based on the SBCCSP I algorithm were on par with the schemes of CSP, MBCSP and FBCSP on average accuracies of each target subject, while the schemes of SBCCSP II and SBCCSP III algorithms far outperformed other schemes. The SBCCSP III scheme performed best in the classifications for Subject F of the saline experiments with the 1000ms data segment, and the average accuracy reached 99.38% when the ratio was 30%.

Combined with the classification results for all subjects, the proposed SBCCSP I and SBCCSP II/III algorithms have been validated with slightly better and significantly better feature extraction and convergence speed than CSP, MBCSP, and FBCSP algorithms. Moreover, the excellent cross-subject adaptation for lower limb classification of TA-SBCCSP II/III schemes has also been shown in the performances.

Based on the experimental results, the enhancement of three SBCCSP algorithms to the cross-subject lower limb MI classification schemes was well demonstrated. In particular, SBCCSP Type II and III algorithms significantly improved the accuracy and reduced the running time. The TA-SBCCSP II/III scheme mostly outperformed TA-SBCCSP I scheme in the experiments because SBCCSP II/III can aggregate all the sub-band features and conduct the comprehensive refinement for the aggregated features to integrate information from all sub-bands, eliminate redundant information and reduce the number of features. Furthermore, the SBCCSP Type III algorithm can perform deep feature refinement of each sub-band to achieve better classification performance than Type II. Since the TA-SBCCSP III scheme achieved the best performance for classification with the data segment size of 500ms and 1000ms, this scheme is the most suitable one for the cross-subject lower limb stepping classification based on stepping-based MI signals.

5 Conclusion and Future Work

5.1 Conclusion

This study investigated the generic cross-subject stepping-based MI classification problem in BCI. As little attention has been paid to refining the extracted features in CSP variants, three novel SBCCSP algorithms were proposed to extract representative features with low redundancy. Based on the SBCCSP algorithms, a cross-subject lower limb MI stepping classification scheme was proposed in this study. The classification scheme consists of data preprocessing, data augmentation, data alignment, SBCCSP algorithm, and deep transfer DTL classifier. The experiments with lower limb stepping MI tasks were designed for six able-bodied subjects with two EEG acquisition devices. There were three labels for the collected data: left leg stepping, right leg stepping, and idle state. Experimental results demonstrated that the schemes adopting the SBCCSP had superior classification performances in accuracy and running time than those adopting other CSP algorithms. The results illustrated that the SBCCSP algorithms had better feature refining and redundancy removal abilities.

5.2 Future Work

The proposed high-performance scheme fills the current gap in the cross-subject lower limb MI classification problem with stepping-based MI signals. The scheme adopting the SBCCSP can be adopted as a generic model for cross-subject lower limb stepping MI classification with high performance. Furthermore, the proposed scheme can contribute to the future development of generic lower limb BCI systems for auxiliary and rehabilitation applications. Notably, manually labeled EEG data often are expensive and time-consuming to collect, clean, and debug. Therefore, the semi-supervised learning mechanism can be added in future work to train the scheme with the few labeled data and a large amount of unlabeled data. Moreover, further improvement can be achieved by adopting an adversarial DTL classifier into the scheme to learn from realistic samples and produce numerous forged samples for training [56].

Acknowledgments

The authors would like to gratefully acknowledge the support from Prof. Eng Gee Lim and Dr. Mark Leach of Suzhou Municipal Key Laboratory for Broadband Wireless Technologies.

References

[1] Y. Tang, Z. Wang, H. Gao, S. Swift, and J. Kurths, "A constrained evolutionary computation method for detecting controlling regions of cortical networks," *IEEE/ACM Transactions on Computational Biology and Bioinformatics*, vol. 9, no. 6, pp. 1569–1581, 2012.

[2] Q. Noirhomme, R. I. Kitney, and B. Macq, "Single-trial EEG source reconstruction for brain–computer interface," *IEEE Transactions on Biomedical Engineering*, vol. 55, no. 5, pp. 1592–1601, 2008.

[3] Y. He, D. Eguren, J. M. Azorín, R. G. Grossman, T. P. Luu, and J. L. Contreras-Vidal, "Brain–machine interfaces for controlling lower-limb powered robotic systems," *Journal of Neural Engineering*, vol. 15, no. 2, 2018, art. no. 021004.

[4] M. Huang, Y. Zheng, J. Zhang, B. Guo, C. Song, and R. Yang, "Design of a hybrid brain-computer interface and virtual reality system for post-stroke rehabilitation," *IFAC-PapersOnLine*, vol. 53, no. 2, pp. 16010–16015, 2020.

[5] Z. Wan, R. Yang, M. Huang, N. Zeng, and X. Liu, "A review on transfer learning in EEG signal analysis," *Neurocomputing*, vol. 421, pp. 1–14, 2021.

[6] Z. Wan, R. Yang, M. Huang, W. Liu and N. Zeng, "EEG fading data classification based on improved manifold learning with adaptive neighborhood selection," *Neurocomputing*, 2021.

[7] D. Wei, Z. Li, Q. Wei, H. Su, B. Song, W. He, and J. Li, "Human-in-the-loop control strategy of unilateral exoskeleton robots for gait rehabilitation," *IEEE Transactions on Cognitive and Developmental Systems*, vol. 13, no. 1, pp. 57–66, 2019.

[8] A. Kline, C. G. Ghiroaga, D. Pittman, B. Goodyear, and J. Ronsky, "EEG differentiates left and right imagined lower limb movement," *Gait & Posture*, vol. 84, pp. 148–154, 2021.

[9] Y. Liu, W. Su, Z. Li, G. Shi, X. Chu, Y. Kang, and W. Shang, "Motor-imagery-based teleoperation of a dual-arm robot performing manipulation tasks," *IEEE Transactions on Cognitive and Developmental Systems*, vol. 11, no. 3, pp. 414–424, 2018.

[10] M. T. Sadiq, X. Yu, Z. Yuan, M. Z. Aziz, S. Siuly, and W. Ding, "A matrix determinant feature extraction approach for decoding motor and mental imagery EEG in subject specific tasks," *IEEE Transactions on Cognitive and Developmental Systems*, 2020.

[11] Y. Hashimoto and J. Ushiba, "EEG-based classification of imaginary left and right foot movements using beta rebound," *Clinical Neurophysiology*, vol. 124, no. 11, pp. 2153–2160, 2013.

[12] S. Y. Gordleeva, S. A. Lobov, N. A. Grigorev, A. O. Savosenkov, M. O. Shamshin, M. V. Lukoyanov, M. A. Khoruzhko, and V. B. Kazantsev, "Real-time EEG–EMG human–machine interface-based control system for a lower-limb exoskeleton," *IEEE Access*, vol. 8, pp. 84 070–84 081, 2020.

[13] C. Wang, X. Wu, Z. Wang, and Y. Ma, "Implementation of a brain-computer interface on a lower-limb exoskeleton," *IEEE Access*, vol. 6, pp. 38 524–38 534, 2018.

[14] W.-C. Hsu, L.-F. Lin, C.-W. Chou, Y.-T. Hsiao, and Y.-H. Liu, "EEG classification of imaginary lower limb stepping movements based on fuzzy support vector machine with kernel-induced membership function," *International Journal of Fuzzy Systems*, vol. 19, no. 2, pp. 566–579, 2017.

[15] L. Gu, Z. Yu, T. Ma, H. Wang, Z. Li, and H. Fan, "EEG-based classification of lower limb motor imagery with brain network analysis," *Neuroscience*, vol. 436, pp. 93–109, 2020.

[16] M. Tariq, P. M. Trivailo, and M. Simic, "Classification of left and right foot kinaesthetic motor imagery using common spatial pattern," *Biomedical Physics & Engineering Express*, vol. 6, no. 1, 2019, art. no. 015008.

[17] J. Choi, K. T. Kim, J. H. Jeong, L. Kim, S. J. Lee, and H. Kim, "Developing a motor imagery-based real-time asynchronous hybrid BCI controller for a lower-limb exoskeleton," *Sensors*, vol. 20, no. 24, 2020, art. no. 7309.

[18] G. Yu, J. Wang, W. Chen, and J. Zhang, "EEG-based brain-controlled lower extremity exoskeleton rehabilitation robot," in *2017 IEEE International Conference on Cybernetics and Intelligent Systems (CIS) and IEEE Conference on Robotics, Automation and Mechatronics (RAM)*. IEEE, 2017, pp. 763–767.

[19] Y.-H. Liu, L.-F. Lin, C.-W. Chou, Y. Chang, Y.-T. Hsiao, and W.-C. Hsu, "Analysis of electroencephalography event-related desynchronisation and synchronisation induced by lower-limb stepping motor imagery," *Journal of Medical and Biological Engineering*, vol. 39, no. 1, pp. 54–69, 2019.

[20] Y. Chen, R. Yang, M. Huang, Z. Wang, and X. Liu, "Single-source to single-target cross-subject motor imagery classification based on multisubdomain adaptation network," *IEEE Transactions on Neural Systems and Rehabilitation Engineering*, vol. 30, pp. 1992–2002, 2022.

[21] P. Mathur and V. K. Chakka, "Graph signal processing based cross-subject mental task classification using multi-channel EEG signals," *IEEE Sensors Journal*, vol. 22, no. 8, pp. 7971–7978, 2022.

[22] Z. Chang, C. Zhang, and C. Li, "Motor imagery EEG classification based on transfer learning and multi-scale convolution network," *Micromachines*, vol. 13, no. 6, 2022, art. no. 927.

[23] K. Samanta, S. Chatterjee, and R. Bose, "Cross-subject motor imagery tasks EEG signal classification employing multiplex weighted visibility graph and deep feature extraction," *IEEE Sensors Letters*, vol. 4, no. 1, pp. 1–4, 2019.

[24] W. Hang, W. Feng, R. Du, S. Liang, Y. Chen, Q. Wang, and X. Liu, "Cross-subject EEG signal recognition using deep domain adaptation network," *IEEE Access*, vol. 7, pp. 128 273–128 282, 2019.

[25] T. Duan, M. A. Shaikh, M. Chauhan, J. Chu, R. K. Srihari, A. Pathak, and S. N. Srihari, "Meta learn on constrained transfer learning for low resource cross subject EEG classification," *IEEE Access*, vol. 8, pp. 224 791–224 802, 2020.

[26] V. Gupta, M. D. Chopda, and R. B. Pachori, "Cross-subject emotion recognition using flexible analytic wavelet transform from EEG signals," *IEEE Sensors Journal*, vol. 19, no. 6, pp. 2266–2274, 2018.

[27] M. Jiménez-Guarneros and P. Gómez-Gil, "Custom domain adaptation: A new method for cross-subject, EEG-based cognitive load recognition," *IEEE Signal Processing Letters*, vol. 27, pp. 750–754, 2020.

[28] M. Grosse-Wentrup and M. Buss, "Multiclass common spatial patterns and information theoretic feature extraction," *IEEE Transactions on Biomedical Engineering*, vol. 55, no. 8, pp. 1991–2000, 2008.

[29] S.-L. Wu, Y.-T. Liu, T.-Y. Hsieh, Y.-Y. Lin, C.-Y. Chen, C.-H. Chuang, and C.-T. Lin, "Fuzzy integral with particle swarm optimization for a motor-imagery-based brain–computer interface," *IEEE Transactions on Fuzzy Systems*, vol. 25, no. 1, pp. 21–28, 2016.

[30] K. P. Thomas, C. Guan, C. T. Lau, A. P. Vinod, and K. K. Ang, "A new discriminative common spatial pattern method for motor imagery brain–computer interfaces," *IEEE Transactions on Biomedical Engineering*, vol. 56, no. 11, pp. 2730–2733, 2009.

[31] Q. Novi, C. Guan, T. H. Dat, and P. Xue, "Sub-band common spatial pattern (SBCSP) for brain-computer interface," in *2007 3rd International IEEE/EMBS Conference on Neural Engineering*. IEEE, 2007, pp. 204–207.

[32] K. K. Ang, Z. Y. Chin, H. Zhang, and C. Guan, "Filter bank common spatial pattern (FBCSP) in brain-computer interface," in *2008 IEEE International Joint Conference on Neural Networks (IEEE World Congress on Computational Intelligence)*. IEEE, 2008, pp. 2390–2397.

[33] Z. Wan, R. Yang, M. Huang, F. E. Alsaadi, M. M. Sheikh, and Z. Wang, "Segment alignment based cross-subject motor imagery classification under fading data," *Computers in Biology and Medicine*, 2022, doi: 10.1016/j.compbiomed.2022.106267.

[34] H. Ramoser, M.-G. Johannes, and P. Gert, "Optimal spatial filtering of single trial EEG during imagined hand movement," *IEEE Transactions on Rehabilitation Engineering*, vol. 8, no. 4, pp. 441–446, 2000.

[35] Y. Wang, S. Gao, and X. Gao, "Common spatial pattern method for channel selelction in motor imagery based brain-computer interface," in *2005 IEEE Engineering in Medicine and Biology 27th Annual Conference*. IEEE, 2006, pp. 5392–5395.

[36] L. Wang, Z. Yan, and Y. Liu, "Temporal-spatial-frequency feature selection of brain-computer interface based on BQPSO," in *2020 9th International Conference on Bioinformatics and Biomedical Science*, 2020, pp. 71–76.

[37] F. Qu, X. Zhao, X. Wang and E. Tian, "Probabilistic-constrained distributed fusion filtering for a class of time-varying systems over sensor networks: a torus-event-triggering mechanism", *International Journal of Systems Science*, vol. 53, no. 6, pp. 1288–1297, 2022.

[38] L. Liu, L. Ma, J. Zhang and Y. Bo, "Distributed non-fragile set-membership filtering for nonlinear systems under fading channels and bias injection attacks", *International Journal of Systems Science*, vol. 52, no. 6, pp. 1192–1205, 2021.

[39] J. Mao, Y. Sun, X. Yi, H. Liu and D. Ding, "Recursive filtering of networked nonlinear systems: A survey, *International Journal of Systems Science"*, vol. 52, no. 6, pp. 1110–1128, 2021.

[40] A. Subasi and M. I. Gursoy, "EEG signal classification using PCA, ICA, LDA and support vector machines," *Expert Systems with Applications*, vol. 37, no. 12, pp. 8659–8666, 2010.

[41] I. Winkler, S. Haufe, and M. Tangermann, "Automatic classification of artifactual ICA-components for artifact removal in EEG signals," *Behavioral and Brain Functions*, vol. 7, no. 1, pp. 1–15, 2011.

[42] T.-H. Z. Cheng, S. C. Creel, and J. R. Iversen, "How do you feel the rhythm: Dynamic motor-auditory interactions are involved in the imagination of hierarchical timing," *Journal of Neuroscience*, vol. 42, no. 3, pp. 500–512, 2022.

[43] X. Zhang, Q. She, Y. Chen, W. Kong, and C. Mei, "Sub-band target alignment common spatial pattern in brain-computer interface," *Computer Methods and Programs in Biomedicine*, vol. 207, 2021, art. no. 106150.

[44] D. Wu, Y. Xu, and B.-L. Lu, "Transfer learning for EEG-based brain–computer interfaces: A review of progress made since 2016," *IEEE Transactions on Cognitive and Developmental Systems*, vol. 14, no. 1, pp. 4–19, 2020.

[45] W. Li, W. Huan, B. Hou, Y. Tian, Z. Zhang, and A. Song, "Can emotion be transferred?–a review on transfer learning for EEG-based emotion recognition," *IEEE Transactions on Cognitive and Developmental Systems*, 2021.

[46] W. Zhang and D. Wu, "Lightweight source-free transfer for privacy-preserving motor imagery classification," *IEEE Transactions on Cognitive and Developmental Systems*, 2022.

[47] M. Wei, R. Yang, and M. Huang, "Motor imagery EEG signal classification based on deep transfer learning," in *2021 IEEE 34th International Symposium on Computer-Based Medical Systems (CBMS)*. IEEE, 2021, pp. 85–90.

[48] N. Zeng, P. Wu, Z. Wang, H. Li, W. Liu, and X. Liu, "A small-sized object detection oriented multi-scale feature fusion approach with application to defect detection," *IEEE Transactions on Instrumentation and Measurement*, vol. 71, pp. 1–14, 2022.

[49] R. J. Seitz, K. M. Stephan, and F. Binkofski, "Control of action as mediated by the human frontal lobe," *Executive Control and the Frontal Lobe: Current Issues*, pp. 71–80, 2000.

[50] P. Beleza and J. Pinho, "Frontal lobe epilepsy," *Journal of Clinical Neuroscience*, vol. 18, no. 5, pp. 593–600, 2011.

[51] M. Wieser, J. Haefeli, L. Bütler, L. Jäncke, R. Riener, and S. Koeneke, "Temporal and spatial patterns of cortical activation during assisted lower limb movement," *Experimental Brain Research*, vol. 203, no. 1, pp. 181–191, 2010.

[52] S. B. Lim, D. R. Louie, S. Peters, T. Liu-Ambrose, L. A. Boyd, and J. J. Eng, "Brain activity during real-time walking and with walking interventions after stroke: a systematic review," *Journal of NeuroEngineering and Rehabilitation*, vol. 18, no. 1, pp. 1–19, 2021.

[53] R. W. Homan, J. Herman, and P. Purdy, "Cerebral location of international 10–20 system electrode placement," *Electroencephalography and Clinical Neurophysiology*, vol. 66, no. 4, pp. 376–382, 1987.

This article has been accepted for publication in a future issue of this journal, but has not been fully edited. Content may change prior to final publication. Citation information: DOI10.1109/TCDS.2023.3338460, IEEE Transactions on Cognitive and Developmental Systems

[54] A. Delorme and S. Makeig, "EEGLAB: an open source toolbox for analysis of single-trial EEG dynamics including independent component analysis," *Journal of Neuroscience Methods*, vol. 134, no. 1, pp. 9–21, 2004.
[55] H. He and D. Wu, "Transfer learning for brain–computer interfaces: A Euclidean space data alignment approach," *IEEE Transactions on Biomedical Engineering*, vol. 67, no. 2, pp. 399–410, 2019.
[56] J. Sun, Z. Wang, H. Yu, S. Zhang, J. Dong, and P. Gao, "Two-stage deep regression enhanced depth estimation from a single RGB image," *IEEE Transactions on Emerging Topics in Computing*, vol. 10, no. 2,, pp. 719–727, 2022.

Mingnan Wei received the M.Res. degree and B.Eng. degree from School of Electrical Engineering, Electronics & Computer Science, University of Liverpool, Liverpool, U.K in 2022 and 2020 respectively. He is currently pursuing the Ph.D. degree in Hong Kong University of Science and Technology (Guangzhou). His research interests include machine learning and biomedical signal analysis.

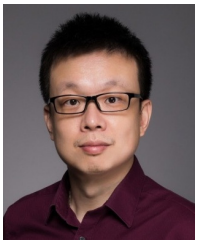

Rui Yang received the B.Eng. degree in Computer Engineering and the Ph.D. degree in Electrical and Computer Engineering from National University of Singapore in 2008 and 2013 respectively.

He is currently an Associate Professor in the School of Advanced Technology, Xi'an Jiaotong-Liverpool University, Suzhou, China, and an Honorary Lecturer in the Department of Computer Science, University of Liverpool, Liverpool, United Kingdom. His research interests include machine learning based data analysis and applications. He is the author or co-author of several technical papers and also a very active reviewer for many international journals and conferences. Dr. Yang is currently serving as an Associate Editor for Neurocomputing and International Journal of Network Dynamics and Intelligence.

Mengjie Huang received the Ph.D. degree from National University of Singapore in 2014, and the B.Eng degree from Sichuan University in 2009.

She is now an Assistant Professor in the Design School, Xi'an Jiaotong-Liverpool University, Suzhou, China. Dr Huang's current research interests include human-computer interaction and applications.

Jiaying Ni received the B.A. degree in Product Design from Zhengzhou University of Light Industry, Zhengzhou, China, in 2020. She is currently pursuing the M.Des. degree in Department of Civil Engineering and Industrial Design, University of Liverpool, Liverpool, U.K. Her research interests include design psychology and human-machine interaction.

Zidong Wang (Fellow, IEEE) received the B.Sc. degree in mathematics in 1986 from Suzhou University, Suzhou, China, the M.Sc. degree in applied mathematics and the Ph.D. degree in electrical engineering both from Nanjing University of Science and Technology, Nanjing, China, in 1990 and 1994, respectively.

He is currently Professor of Dynamical Systems and Computing in the Department of Computer Science, Brunel University London, U.K. From 1990 to 2002, he held teaching and research appointments in universities in China, Germany and the UK. Prof. Wang's research interests include dynamical systems, signal processing, bioinformatics, control theory and applications. He has published more than 700 papers in international journals. He is a holder of the Alexander von Humboldt Research Fellowship of Germany, the JSPS Research Fellowship of Japan, William Mong Visiting Research Fellowship of Hong Kong.

Prof. Wang serves (or has served) as the Editor-in-Chief for *International Journal of Systems Science*, the Editor-in-Chief for *Neurocomputing*, the Editor-in-Chief for *Systems Science & Control Engineering*, and an Associate Editor for 12 international journals, including IEEE TRANSACTIONS ON AUTOMATIC CONTROL, IEEE TRANSACTIONS ON CONTROL SYSTEMS TECHNOLOGY, IEEE TRANSACTIONS ON NEURAL NETWORKS, IEEE TRANSACTIONS ON SIGNAL PROCESSING, and IEEE TRANSACTIONS ON SYSTEMS, MAN, AND CYBERNETICS–PART C. He is a Member of the Academia Europaea, a Member of the European Academy of Sciences and Arts, an Academician of the International Academy for Systems and Cybernetic Sciences, a Fellow of the IEEE, a Fellow of the Royal Statistical Society, and a member of program committee for many international conferences.

Xiaohui Liu received the B.Eng. Degree in Computing from Hohai University, Nanjing, China, in 1982 and the Ph.D. degree in Computer Science from Heriot-Watt University, Edinburgh, UK, in 1988. He is currently a Professor of Computing at Brunel University London where he conducts research in AI and intelligent data analysis, with applications in diverse areas including biomedicine and engineering.